Cold Collisions of OH($^2\Pi$) Molecules with He Atoms in External Fields†

Z. Pavlovic,‡,§ T. V. Tscherbul,*,‡,∥ H. R. Sadeghpour,‡ G. C. Groenenboom,⊥ and A. Dalgarno‡,∥

ITAMP, Harvard-Smithsonian Center for Astrophysics, Cambridge, Massachusetts 02138, Department of Physics, University of Connecticut, Storrs, Connecticut 06269, Harvard-MIT Center for Ultracold Atoms, Cambridge, Massachusetts 02138, and Theoretical Chemistry, Institute for Molecules and Materials, Radboud University Nijmegen, Heyendaalseweg 135, 6525 AJ Nijmegen, The Netherlands

Received: May 14, 2009; Revised Manuscript Received: August 3, 2009

We present rigorous quantum calculations for low-temperature collisions of OH($^2\Pi$) molecules with He atoms in the presence of external electric and magnetic fields. We show that electric fields of less than 15 kV/cm can be used to enhance the probability for Stark relaxation in collisions of OH (F_1, $J = 3/2$, $M = 3/2$, f) molecules by 3 orders of magnitude. The inelastic cross sections display a pronounced resonance structure as a function of the electric field strength. We find that collisions of rotationally excited OH molecules become less sensitive to electric fields with increasing rotational excitation. The calculated total cross sections for ^{4}He−OH are dominated by elastic scattering, increase monotonically with decreasing collision energy, and show no rapid variations near thresholds, at variance with recent experimental observations (Sawyer et al. *Phys. Rev. Lett.* **2008**, *101*, 203203).

I. Introduction

Understanding the mechanisms of inelastic collisions and chemical reactions of open-shell molecules is a necessary prerequisite to quantitative modeling in atmospheric chemistry,[1] combustion,[2] and astrochemistry.[3] The main theoretical challenge in describing these processes comes from the complicated energy level structure of molecules in degenerate electronic states, which is perturbed by fine, hyperfine, spin−rotation, spin−spin, and Coriolis interactions.[4] Therefore, in addition to purely rotational energy transfer, collisions of molecular radicals may lead to spin depolarization and nonadiabatic mixing of different electronic states.[5−10] Such transitions are often determined by strict propensity rules and provide a wealth of valuable information about the nonadiabatic effects in chemical dynamics[11] and photodissociation.[12] In particular, the probability of the chemical reaction of Cl atoms with H_2 molecules at low collision energies depends sensitively on the fine-structure state of the Cl atom.[13] The Λ-doublet changing transitions, whose efficiency is determined by collisional propensity rules, are responsible for pumping of interstellar masers.[3] The interactions of $^2\Pi$-state molecules with dc electric fields can be used to manipulate molecular beams[14] and study the effects of orientation and alignment on molecular collisions and chemical reactions.[6]

Recent advances in experimental techniques to cool and trap neutral molecules and molecular ions at milli-Kelvin temperatures[15,16] have generated a renewed interest in low-energy collisions of polar molecules in the presence of external electromagnetic fields.[17] The techniques such as cryogenic cooling[18] and Stark deceleration[19] rely on the interactions with electromagnetic fields to manipulate molecular trajectories. Polar molecules in electronic states of Π symmetry have electric and magnetic moments, so their motion can be controlled by both electric and magnetic fields. The energy levels of molecules in Π electronic states depend linearly on the electric field strength above a few kV/cm, facilitating electric field manipulation.

The OH radical is of fundamental importance to astrophysics,[3] atmospheric chemistry,[1] and precision spectroscopy.[20] The ground electronic state of OH is of $^2\Pi$ symmetry, so the molecule can be efficiently manipulated with time-varying electric fields. In a series of groundbreaking experiments, Meijer and co-workers combined Stark deceleration[14] with electrostatic trapping[19] to carry out high-resolution spectroscopic measurements of the radiative lifetime of OH ($v = 1$)[21] and study cold collisions of OH molecules with Xe atoms in crossed molecular beams.[22] Similar measurements were reported for the metastable CO($^3\Pi$), NH($^1\Delta$), and ground-state ammonia molecules.[14] Electrostatic traps confine molecules in the highest-energy Stark level of the ground rotational state. Collisions with background gas atoms may lead to depopulation of the Stark level followed by trap loss and defocusing. Understanding the mechanisms of collision-induced Stark relaxation is therefore essential for minimizing trap losses and optimizing evaporative cooling of molecules in electrostatic traps.[24,25]

The cross sections for electronic and rotational energy transfer in collisions of $^2\Pi$ molecules with rare gas atoms were measured in a number of experiments.[5−9,22,23] In particular, collisions of OH molecules with He and Ar atoms were studied in crossed molecular beams[5] and strong steric effects were observed in the presence of an external electric field.[6] The rate constants for rotational depolarization of OH molecules in collisions with He and Ar atoms have recently been measured by McKendrick and co-workers[7,8] and Brouard et al.[9] Gilijamse et al. measured the cross sections for rotational excitation in Xe−OH collisions as functions of collision energy near threshold.[22] Sawyer et al. measured total cross sections for collisions of magnetically trapped OH molecules with He atoms and D_2 molecules[23] as a function of collision energy. A variation of the cross sections

† Part of the "Vincenzo Aquilanti Festschrift".

* To whom correspondence should be addressed. E-mail: tshcherb@cfa.harvard.edu.

‡ Harvard-Smithsonian Center for Astrophysics.

§ University of Connecticut.

∥ Harvard-MIT Center for Ultracold Atoms.

⊥ Radboud University Nijmegen.

10.1021/jp904512r
Published on Web 08/27/2009

at collision energies between 70 and 130 cm^{-1} was observed and attributed to a quantum mechanical threshold effect.[23]

The formal quantum-mechanical theory for collisions of Π-state molecules with atoms was developed by Klar,[27] Shapiro and Kaplan,[28] and Alexander.[29] Alexander and co-workers applied the theory to calculate the cross sections for transitions between fine-structure and Λ-doublet levels of OH, NO, CN, and CH molecules in collisions with structureless particles.[30−32] Dagdigian and Alexander proposed a rigorous formalism for collisional depolarization of $^2\Pi$ molecules in collisions with He atoms.[26] Avdeenkov and Bohn analyzed the effects of electric fields on the collision dynamics of OH molecules and discovered new field-linked molecular states.[33−35] Lara et al. developed a theoretical approach taking into account the nonadiabatic and hyperfine interactions to calculate the rate constants for inelastic relaxation in collisions of OH molecules with Rb atoms.[24,25] González-Sánchez et al. analyzed propensity rules for state-to-state inelastic transitions in ultracold He−OH collisions.[36]

We have recently developed a fully quantum-mechanical theory for collisions of $^2\Pi$ molecules with structureless atoms in the presence of external electromagnetic fields.[37] We applied the theory to calculate the cross sections and rate constants for elastic energy transfer and spin relaxation in collisions of OH molecules in the ground rotational state with helium atoms. We demonstrated a general mechanism for suppressing collision-induced inelastic relaxation of $^2\Pi$ molecules in high-electric-field-seeking *e*-parity states based on eliminating magnetic relaxation channels by shifting them above the collision threshold.[37]

In this paper, we present a theoretical analysis of low-temperature collisions of He atoms with OH and CH molecules in *low-electric-field-seeking* states of *f*-symmetry. A brief account of the theoretical methodology[37] is given in section II. Our results for elastic scattering and Stark relaxation in He−OH collisions over a wide range of temperatures (1 mK to 200 K) and electric fields (0−150 kV/cm) are presented in section IIIA and B.[38] In section IIIC, we compare our calculations with experimental data.[23] Section IV summarizes the results.

II. Theory

In this section, we briefly outline the quantum mechanical theory for collisions of molecules in $^2\Pi$ electronic states with $^1S_0$ atoms in the presence of external electric and magnetic fields.[37] The collision problem is described by the Hamiltonian

$$\hat{H} = -\frac{1}{2\mu R}\frac{\partial^2}{\partial R^2}R + \frac{\hat{l}^2}{2\mu R^2} + \hat{V}(R, r, \theta) + \hat{H}_{\mathrm{mol}} \quad (1)$$

where $r = |\mathbf{r}|$ is the internuclear distance in the diatomic molecule, $R = |\mathbf{R}|$ is the length of the atom−molecule separation vector, θ is the angle between the vectors $\mathbf{R}$ and $\mathbf{r}$, μ is the atom−molecule reduced mass, and $\hat{l}$ is the orbital angular momentum for the relative motion of the collision partners. Because the fundamental frequency of OH ($\omega = 3569.64\ cm^{-1}$) by far exceeds the energy scale of cold collisions (10^{-3}−200 K), we can assume that the vibrational motion of OH is frozen out, that is, $r = r_e$, where $r_e = 1.226$ Å is the equilibrium distance of OH in the ground electronic state. The Hamiltonian $\hat{H}_{\mathrm{mol}}$ determines the energy level structure of the molecule in the presence of external fields. The effective Hamiltonian for the ground vibrational state can be written as[37,39,40]

$$\hat{H}_{\mathrm{mol}} = B_e[\hat{J}^2 - 2\hat{J}_z^2 - \hat{J}_+\hat{S}_- - \hat{J}_-\hat{S}_+] + (A + 2B_e)\hat{L}_z\hat{S}_z + \hat{H}_B + \hat{H}_E + \hat{H}_\Lambda \quad (2)$$

where B_e is the rotational constant of the molecule, $\hat{J} = \hat{N} + \hat{L} + \hat{S}$ is the total angular momentum, $\hat{N}$ is the rotational angular momentum of the nuclei, $\hat{L}$ is the electronic orbital angular momentum, and $\hat{S}$ is the electron spin. The first two terms in eq 2 represent the rotational and spin−orbit (SO) Hamiltonians expressed through the ladder operators $\hat{J}_\pm\hat{S}_\mp$ and the molecule-fixed projection of the total angular momentum $\hat{J}_z$. We neglect the weak hyperfine interaction due to the H nuclear spin.[37] The term $A\hat{L}_z\hat{S}_z$ accounts for the diagonal part of the SO interaction parametrized by the SO constant A. The off-diagonal part of the SO interaction mixes the ground ($^2\Pi$) and excited ($^2\Sigma$) electronic states, leading to Λ-doubling effects described by the Hamiltonian $\hat{H}_\Lambda$.[37] Also included in eq 2 is the interaction of the permanent electric dipole moment of the molecule d with a dc electric field E

$$\hat{H}_E = -Ed\cos\theta_r \quad (3)$$

which depends on the orientation angle θ_r of the molecular axis in the space-fixed frame. The interaction with magnetic fields is given by

$$\hat{H}_B = \mu_0 B(\hat{L} + 2\hat{S}) \cdot \hat{B} \quad (4)$$

where B is the field strength and μ_0 is the Bohr magneton. We assume that the electric and magnetic fields are coaligned along the space-fixed z-axis.[41] Changing the orientation of the quantization axes does not alter the collision dynamics except near infrequently occurring avoided crossings.[42]

The eigenfunctions of the Hamiltonian (2) can be expanded in parity-adapted Hund's case (a) basis functions

$$|JM\bar{\Omega}\epsilon\rangle = \frac{1}{\sqrt{2}}[|JM\bar{\Omega}\rangle|\Lambda = 1, \Sigma = \bar{\Omega} - 1\rangle + \epsilon(-)^{J-1/2}|JM - \bar{\Omega}\rangle|\Lambda = -1, \Sigma = -\bar{\Omega} + 1\rangle] \quad (5)$$

where the primitive case (a) functions are

$$|JM\Omega\rangle|\Lambda\Sigma\rangle = \left(\frac{2J+1}{4\pi}\right)^{1/2} D^{J*}_{M\Omega}(\chi_r, \theta_r, 0)|\Lambda\Sigma\rangle \quad (6)$$

Here, M and Ω are the projections of the total angular momentum J on the space-fixed and molecule-fixed quantization axes, respectively, $D^{J*}_{M\Omega}$ is the Wigner D-function, and $|\Lambda\Sigma\rangle$ is the electronic wave function. The z-axis of the molecule-fixed coordinate frame coincides with that of the diatomic molecule, whose orientation in the space-fixed frame is specified by two Euler angles χ_r and θ_r. For $^2\Pi$ electronic states, the molecule-fixed projections of $\hat{L}$ and $\hat{S}$ are $\Lambda = \pm 1$ and $\Sigma = \pm 1/2$, so the parity-adapted basis functions are characterized by the absolute value of $\bar{\Omega} = 1/2, 3/2$. The parity quantum number $\epsilon = \pm 1$ in eq 5 characterizes the symmetry of the basis functions with respect to inversion. For an isolated $^2\Pi$ molecule in the absence of external fields, ϵ is conserved, but intermolecular interactions and electric fields break the inversion symmetry and couple the states with different ϵ. In the following, we will adhere to the spectroscopic *e/f* notation based on whether $\epsilon(-1)^{J-1/2} = +1$

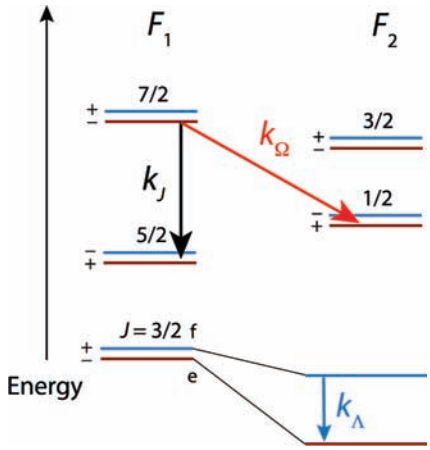

Figure 1. Schematic representation of the energy levels of OH in the absence of external fields. The individual Λ-doublet sublevels are labeled according to their inversion parity $\epsilon = \pm$. The *e*/*f* notation is illustrated for the F_1, $J = 3/2$ energy level. Also shown are different pathways for collision-induced inelastic relaxation: fine-structure ($k_{\bar{\Omega}}$), rotational (k_J), and Λ-doublet changing (k_Λ).

(*e*-states) or −1 (*f*-states). The labels *f* and *e* are convenient because they always correspond to the upper and lower components of a Λ-doublet, unlike the parity indexes ϵ, which alternate with *J* (see Figure 1).

The matrix elements of the Hamiltonian (2) in the basis (5) can be evaluated as described in our previous work.[37] The eigenstates of the real molecule can be written as linear combinations of Hund's case (a) basis functions

$$|\gamma\rangle = \sum_{J,M,\bar{\Omega},\epsilon} C_{JM\bar{\Omega}\epsilon,\gamma}|JM\bar{\Omega}\epsilon\rangle \quad (7)$$

where the field-dependent coefficients $C_{JM\bar{\Omega}\epsilon,\gamma}$ can either be obtained by numerical diagonalization of the Hamiltonian matrix or estimated using perturbation theory. The projection of the total angular momentum of the molecule on the field axis *M* is rigorously conserved. In the following, we will use *M* to label the field-dressed molecular states (see, e.g., Figure 2).

In order to solve the scattering problem, we expand the total wave function of the atom−molecule system as[37]

$$\Psi = \frac{1}{R}\sum_{\beta} F_\beta(R)\psi_\beta(\hat{R},\hat{r}) \quad (8)$$

where

$$\psi_\beta(\hat{R},\hat{r}) = |JM\bar{\Omega}\epsilon\rangle|lm_l\rangle \quad (9)$$

are the uncoupled angular basis functions composed of direct products of Hund's case (a) functions (5) and the spherical harmonics $|lm_l\rangle$ describing the relative motion of the collision partners in the space-fixed coordinate frame. In eq 8, β is used as a collective index for $\{J,M,\bar{\Omega},\epsilon,l,m_l\}$. When substituted into the Schrödinger equation, the expansion (8) yields a set of close-coupled (CC) differential equations

$$\left[\frac{d^2}{dR^2} + 2\mu E\right]F_\beta(R) = 2\mu\sum_{\beta'}\langle\psi_\beta(\hat{R},\hat{r})|\hat{V}(R,\theta) + \frac{\hat{l}^2}{2\mu R^2} + \hat{H}_{mol}|\psi_{\beta'}(\hat{R},\hat{r})\rangle F_{\beta'}(R) \quad (10)$$

The interaction of a $^2\Pi$ molecule with a structureless atom is characterized by two potential energy surfaces (PESs) of A' and A'' symmetries.[29] In this work, we use the most recent *ab initio* interaction potentials calculated by Lee et al. using the partially spin-restricted coupled cluster method with single and double excitations and noniterated triples [RCCSD(T)] with an aug-cc-pVTZ one-electron basis set extended with bond functions.[43] The matrix elements of the interaction potentials in eq 10 can be readily evaluated from their expansions in associated Legendre polynomials as described in detail elsewhere.[37,44]

After transforming the asymptotic wave function to the field-dressed scattering basis

$$|\gamma\rangle|lm_l\rangle \quad (11)$$

with $|\gamma\rangle$ given by eq 7, the scattering *S*-matrix elements can be determined by analyzing the asymptotic form of the solutions $F_{\gamma lm_l}(R)$.[41] The cross sections for elastic energy transfer and inelastic scattering for a given collision energy E_{coll} and electric field strength are given in terms of the *S*-matrix elements as[37,41]

$$\sigma_{\gamma\to\gamma'} = \frac{\pi}{k_\gamma^2}\sum_{M_{tot}}\sum_{l,m_l}\sum_{l',m'_l}|\delta_{\gamma\gamma'}\delta_{ll'}\delta_{m_l,m'_l} - S^{M_{tot}}_{\gamma lm_l;\gamma' l'm'_l}|^2 \quad (12)$$

where ${k_\gamma}^2 = 2\mu(E_{coll} - \epsilon_\gamma)$ is the wave vector for the incoming collision channel γ with internal energy ϵ_γ and E_{coll} is the collision energy. Averaging the cross sections (12) over a Maxwell−Boltzmann distribution of collision energies gives the thermal rate constants for transitions between the individual Stark states.

The CC equations (10) were integrated out to $R_{max} = 60\ a_0$ using the improved log-derivative algorithm[46,47] with a constant step size of 0.1 a_0. The spectroscopic constants of OH used in scattering calculations are (in cm^{-1}): $B_e = 18.55$, $A = -139.273$, $p = 0.235608$, and $q = -0.03877$ (where *p* and *q* are the Λ-doubling parameters).[37,39,40] We use $d = 1.68$ D for the permanent electric dipole moment of OH in the $v = 0$ vibrational state.[35,45] The basis set expansion included the rotational states up to $J_{max} = 11/2$ and partial waves up to $l_{max} = 5$. In order to make calculations at higher collision energies feasible, we reduced the basis set to $J_{max} = 7/2$ and augmented it with partial waves up to $l_{max} = 30$. The resulting cross sections were converged to better than 5%.

III. Results

A. Energy Levels of OH. Figure 1 shows the energy levels of OH in the absence of external fields. The levels in two fine-structure manifolds (F_1 and F_2) are split by the SO interaction. Because the rotational constant of OH is not negligible compared to the SO constant ($|A/B_e| = 7.5$), different values of $\bar{\Omega}$ are coupled by the cross terms $\hat{J}_\pm\hat{S}_\mp$ in eq 2. To illustrate this, we consider the eigenfunctions $|\gamma\rangle$ corresponding to the energy levels shown in Figure 1. The rotational states in the F_1 manifold can be expanded in Hund's case (a) basis functions as follows

$$\left|F_1, J=\frac{3}{2}, M, \epsilon\right\rangle = a_J\left|J=\frac{3}{2}, \bar{\Omega}=\frac{3}{2}, M, \epsilon\right\rangle + b_J\left|J=\frac{3}{2}, \bar{\Omega}=\frac{1}{2}, M, \epsilon\right\rangle \quad (13)$$

where the expansion coefficients a_J and b_J characterize the degree of mixing of different $\bar{\Omega}$-states (in a pure Hund's case (a) molecule, the $\bar{\Omega}$-states are uncoupled). The coefficients (a_J,b_J) are (0.985,0.174) for $J = 3/2$, (0.964,0.264) for $J = 5/2$, and (0.943,0.337) for $J = 7/2$. The F_2 states can be expanded in the same way as in eq 13, with the coefficients given by (0,1) for $J = 1/2$, (−0.174,0.985) for $J = 3/2$, and (−0.266,0.964) for $J = 5/2$. These expressions illustrate that the Coriolis interaction between different $\bar{\Omega}$-states becomes stronger with increasing J. The only exception is the lowest rotational level in the F_2 manifold, which can be represented by a single basis function.

Figure 2 shows the electric field dependence of the energy levels displayed in Figure 1. At small electric fields ($E < E^* = d/\Delta_\Lambda$, where $\Delta_\Lambda = 0.057$ cm^{-1} is the Λ-doublet splitting in OH), the energy levels depend quadratically on the electric field strength. As the electric field approaches the critical value of $E^* \sim 5$ kV/cm, the first-order Stark effect starts to set in. At $E > E^*$, all energy levels exhibit linear Stark shifts. Because the matrix elements of the Λ-doubling Hamiltonian increase linearly with J and so does the splitting Δ_Λ,[4] rotationally excited levels of OH exhibit progressively smaller Stark shifts as J increases. The same conclusion applies to Σ-state molecules[48] because the energy separation between the rotational levels J and $J - 1$ increases linearly with J.

The presence of quasi-degenerate, opposite-parity levels in $^2\Pi$ molecules pushes the onset of the first-order Stark effect to low E-fields (∼10 kV/cm for a typical Λ-doublet splitting of ∼0.1 cm^{-1}). In contrast, the Stark effect in Σ-state molecules is determined by couplings between different *rotational* states. Typical rotational level splittings in most molecules are >10 times larger than the Λ-doublet splittings, so large electric fields are required to induce appreciable Stark shifts in Σ-state molecules. For example, the first-order Stark effect in CaH ($B_e = 6.1$ cm^{-1}) occurs at electric fields above 200 kV/cm, and for the heavy YbF molecule ($B_e = 0.24$ cm^{-1}), this value is about 50 kV/cm. We therefore expect that collisions of Π-state molecules will be more sensitive to electric fields than collisions of Σ-state molecules.

B. Collision Dynamics. Figure 3 shows the cross sections for inelastic relaxation in collisions of OH molecules in different initial rotational states with He atoms as functions of collision energy. The initial states are the fully stretched low-electric-field-seeking states $|F_1, J, M = J, f\rangle$ shown by dashed lines in Figure 2. The total inelastic cross section is the sum of the cross sections for transitions between different fine-structure, rotational, and Stark levels (see Figure 1). At low collision energies, the OH molecules prepared in the ground state $|F_1, J = 3/2, M = 3/2, f\rangle$ can only undergo downward transitions to the Stark states $|F_1, J = 3/2, M', \epsilon'\rangle$. Previous work has shown that the Stark relaxation is determined by the couplings between the different M components of the $J = 3/2$ state induced by the anisotropy of the interaction potential.[37] An important consequence is that the rates for collision-induced Stark relaxation of $^2\Pi$ molecules are large and insensitive to the magnitude of the rotational constant. This is in contrast with the relaxation dynamics of Σ-state molecules, where different M-sublevels of the ground rotational state are uncoupled.[42,48] The large inelastic rates of $^2\Pi$ molecules preclude their sympathetic cooling using ^{3}He buffer gas but can be mitigated by electric fields at temperatures below 0.01 K.[37]

As shown in the upper panel of Figure 3, the cross sections for inelastic transitions in collisions of ground-state OH molecules are highly sensitive to the electric field strength. An electric field of only 7 kV/cm leads to the enhancement of the inelastic cross sections by 2 orders of magnitude at a collision energy of 100 mK. The rate constants for inelastic transitions in He−OH collisions at a temperature of 0.5 K are presented

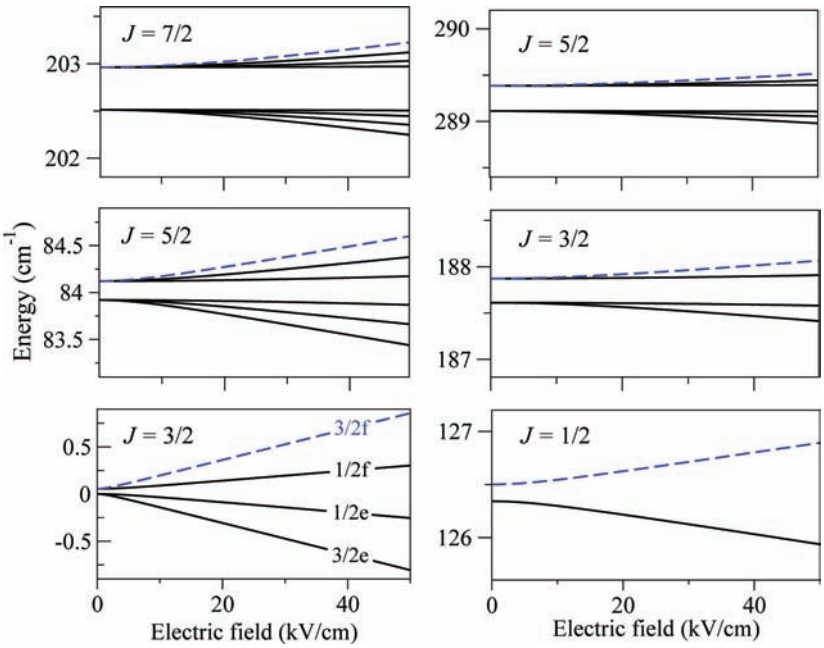

Figure 2. (left panel) Stark levels in the F_1 manifold ($^2\Pi_{3/2}$) vs the applied electric field. (right panel) Stark levels in the F_2 manifold ($^2\Pi_{1/2}$) vs the applied electric field. The initial states for scattering calculations are shown by dashed lines. The Stark levels in different J-manifolds are drawn to scale and labeled for $J = 3/2$ by the absolute value of M. The label e (f) denotes the lower (upper) Λ-doublet in the absence of an electric field. The zero of energy corresponds to the ground state of OH($^2\Pi$) at zero electric and magnetic fields.

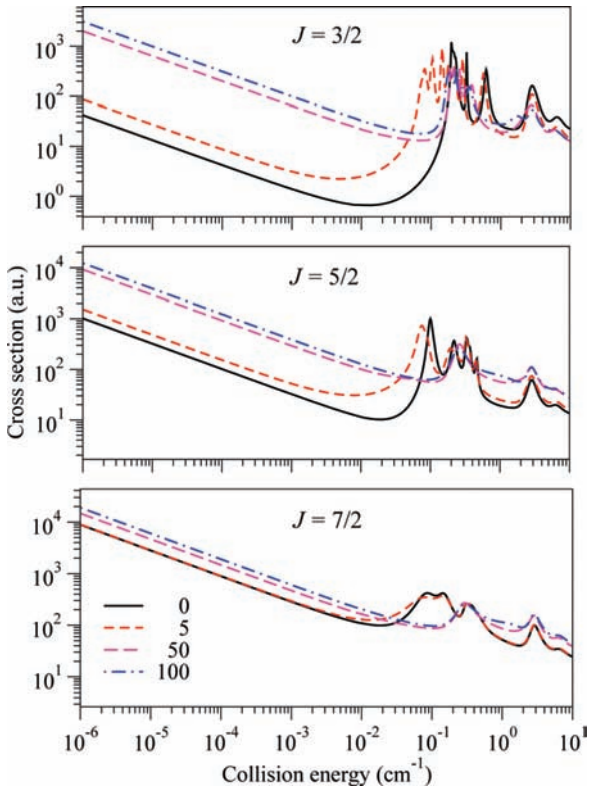

Figure 3. Collision energy dependence of the inelastic cross sections for He−OH($^2\Pi$) collisions. The OH molecules are in the maximally stretched $|F_1, J, M = J, f\rangle$ initial states with $J = 3/2$ (upper panel), $J = 5/2$ (middle panel), and $J = 7/2$ (lower panel). Different curves in each panel refer to different electric fields: zero (full line), 5 kV/cm (short dashed line), 50 kV/cm (long dashed line), and 100 kV/cm (dash−dotted line). The magnetic field is 1 G.

TABLE 1: Total Rate Constants for Inelastic Transitions (in 10^{-12} cm^3/s) from Different Initial Rotational States in the F_1 and F_2 Manifolds for Several Electric Field Strenghts (in kV/cm) at $T = 10$ mK

electric field	0	5	50	100
J		F_1		
3/2	0.02	0.09	0.60	0.89
5/2	0.34	0.98	2.76	3.49
7/2	3.13	3.76	4.43	5.52
J		F_2		
1/2	10.3	10.3	10.8	10.9
3/2	7.67	7.62	8.16	9.15
5/2	6.18	6.22	7.41	8.20
7/2	5.44	5.50	7.44	7.93

in Table 1. The rate constants increase with increasing field strength. The rate constants increase (decrease) with an increase in the initial J value for the F_1 (F_2) manifolds. This is in keeping with the trends observed in Figures 3 and 5.

Figure 4 shows the inelastic cross sections for He−OH as functions of electric field at a collision energy of 10^{-3} cm^{-1}, which corresponds to the s-wave regime in Figure 3. The cross sections display a complicated resonance structure at electric fields between 7 and 30 kV/cm and grow monotonously as the field strength increases past 30 kV/cm. The resonance structure occurs only for collisions of molecules in the ground rotational state $|F_1, J = 3/2\rangle$. For higher rotational states, the availability of many decay channels leads to more efficient inelastic relaxation (cf. Figure 3), leading to suppression of scattering resonances.[49] This tendency is even more pronounced for the initial states in the F_2 manifold. The lower panel of Figure 4 shows that the cross sections for inelastic relaxation out of the $|F_2, J\rangle$ states are almost independent of the electric field.

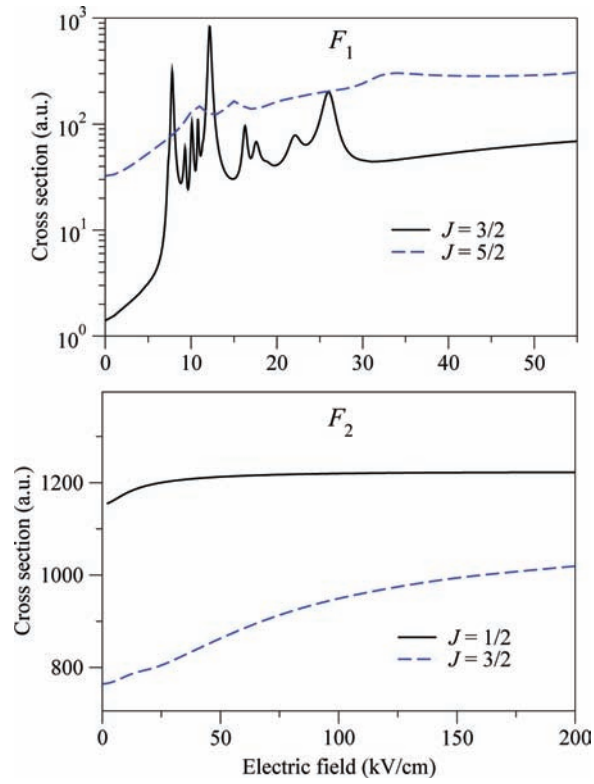

Figure 4. (upper panel) Electric field dependence of the cross sections for inelastic scattering of OH ($F_1, J, M = J, f$) with He for different initial rotational states J. (lower panel) Same as the upper panel but for the OH ($F_2, J, M = J, f$) initial state. The collision energy is 10^{-3} cm^{-1}.

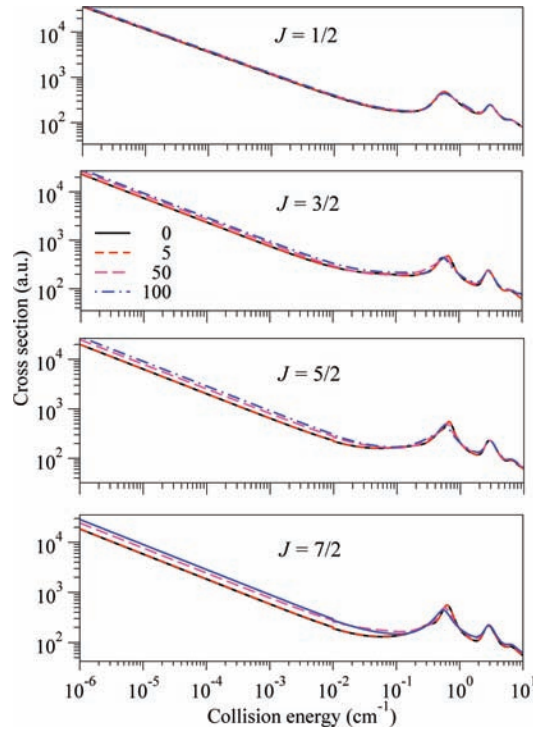

Figure 5. Same as Figure 3 but for the SO excited initial states $|F_2, J, M = J, f\rangle$.

Figure 5 shows the cross sections for inelastic relaxation of rotational states in the F_2 manifold versus collision energy. The corresponding rate constants are presented in Table 1. The

TABLE 2: Rate Constants for $\bar{\Omega}$-Changing, *J*-Changing, and Λ-Changing Transitions (see Figure 1) for Different Electric Field Strengths (in kV/cm)[a]

electric field	0	5	100
		F_1	
k_Λ	0.023	0.115	1.55
k_J	0.312	0.865	1.91
		F_2	
k_Λ	0.033	0.037	0.365
k_J	0.697	0.683	0.593
$k_{\bar{\Omega}}$	6.87	6.90	7.92

[a] The rate constants are given in units of 10^{-12} cm^3/s for the initial states $|F_1, J = 5/2, M = 5/2, f\rangle$ and $|F_2, J = 3/2, M = 3/2, f\rangle$ at $T = 10$ mK.

variation of the cross sections with electric field and initial rotational state is insignificant, because of the presence of efficient fine-structure relaxation channels $|F_2, J\rangle \rightarrow |F_1, J'\rangle$. Indeed, the partial rate constants $k_{\bar{\Omega}}$ presented in Table 2 are 10 times larger than those for *J*-changing and Λ-doublet changing transitions.

Rotational excitation of molecules opens up new relaxation pathways. As shown in Figure 1, the OH molecules in the $J = 7/2$ state can undergo Λ-doublet changing, *J*-changing, and fine-structure transitions. The relative efficiency of these relaxation pathways can be quantified in terms of the partial rate constants k_Λ, k_J, and $k_{\bar{\Omega}}$. The rate constants for these processes are presented in Table 2 for a temperature of 10 mK. The rate constants for Λ-doublet changing transitions increase by 2 orders of magnitude with increasing electric field from 0 to 100 kV/cm. The electric field dependence of the Λ-doublet changing rates for rotationally excited OH molecules is not as dramatic. Similarly, the rate constants for rotational relaxation become less sensitive to the electric field strength with increasing *J*. The collision dynamics of SO-excited OH molecules is determined by the very efficient fine-structure relaxation process $|F_2, J\rangle \rightarrow |F_1, J'\rangle$, which is insensitive to electric field.

In order to elucidate the rich resonance structure shown in Figure 3, it is useful to analyze the cross sections for individual Stark transitions (eq 12). A plot of the state-resolved cross sections versus collision energy for different final states is shown in the upper panel of Figure 6. A few distinct propensity rules are immediately apparent from the figure. The dominant transition $|F_1, J = 3/2, M = 3/2, f\rangle \rightarrow |F_1, J' = 3/2, M' = 1/2, f\rangle$ conserves the inversion parity and corresponds to a minimal change of *M*. However, this propensity rule breaks down near the shape resonance at $E_{\rm coll} \sim 0.2$ cm^{-1}, where the parity-changing transition $|F_1, J = 3/2, M = 3/2, f\rangle \rightarrow |F_1, J' = 3/2, M' = 3/2, e\rangle$ dominates. A closer inspection of Figure 6 shows that, in general, the probability for the transition $|F_1, JM\epsilon\rangle \rightarrow |F_1, J'M'\epsilon'\rangle$ decreases with increasing $\Delta M = M' - M$ and $\Delta\epsilon$. This is in line with the observations made by González-Sánchez et al. in their computational study of ^{4}He−OH collisions.[36]

At zero electric field, the state-to-state cross sections exhibit a series of resonance peaks. Because the total angular momentum projection, $M_{\rm tot} = M + M_l$ is conserved, the inelastic transition $M \rightarrow M'$ must necessarily be accompanied by the transition $m_l \rightarrow m_l + \Delta M$.[37] Thus, even for *s*-wave collisions ($l = 0$), there is always a centrifugal barrier in the outgoing collision channel, which may lead to temporary trapping of the collision partners to form a quasi-bound state (or shape resonance). Outside the *s*-wave regime, the quasibound states can also occur in the incoming collision channel. The lower panel of Figure 6 shows the decomposition of the cross section

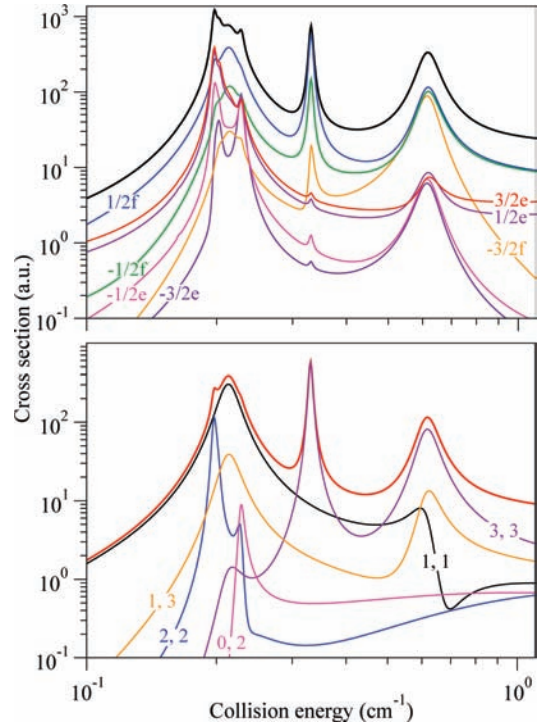

Figure 6. (upper panel) State-to-state cross sections for inelastic scattering of OH (F_1, $J = 3/2$, $M = 3/2$, *f*) with He at zero electric field. The magnetic field is 1 G. (lower panel) Partial wave contributions to the cross section marked as "3/2e" in the upper panel. The magnetic field is 1 G. See text for details.

for the inelastic transition $|F_1, J = 3/2, M = 3/2, f\rangle \rightarrow |F_1, J' = 3/2, M' = 1/2, f\rangle$ into different partial-wave contributions (cf. eq 12)

$$\sigma_{\gamma l \rightarrow \gamma' l'} = \frac{\pi}{k_\gamma^2} \sum_{M_{\rm tot}} \sum_{m_l} \sum_{m_{l'}} \left| \delta_{\gamma\gamma'}\delta_{ll'}\delta_{m_l,m_f} - S^{M_{\rm tot}}_{\gamma l m_l;\gamma' l' m_{l'}} \right|^2 \tag{14}$$

By analyzing the *l*-resolved cross sections as functions of collision energy, each resonance can be assigned the quantum numbers *l* and *l*′. The analysis shows that the broad peak at $E_{\rm coll} \sim 0.65$ cm^{-1} can be identified as an $l = 3$ shape resonance, and the lowest-energy peak is due to an $l = 1$ shape resonance (in these cases, $l' = l$, i.e., the resonances occur in both the incoming and outgoing collision channels). There are also resonances corresponding to the centrifugal barriers in the outgoing collision channel. An example of such a resonance due to the $l = 0 \rightarrow l' = 2$ transition is shown in the lower panel of Figure 6. We note that many of the resonances shown in the lower panel of Figure 6 do not show up in the total cross section because of the averaging, which occurs when different partial wave contributions are added together.

Electric fields couple the opposite parity states ($\Delta\epsilon = \pm 2$), which alters the selection rules for individual Stark transitions. The upper panel of Figure 7 shows the state-to-state inelastic cross sections as functions of collision energy in the presence of an electric field of 5 kV/cm. A comparison with Figure 6 shows that electric fields alter field-free propensity rules in such a way that the incoming collision flux gets redistributed more evenly between different outgoing channels. The absolute values of the cross sections and the number of shape resonances increase considerably compared to the field-free case.

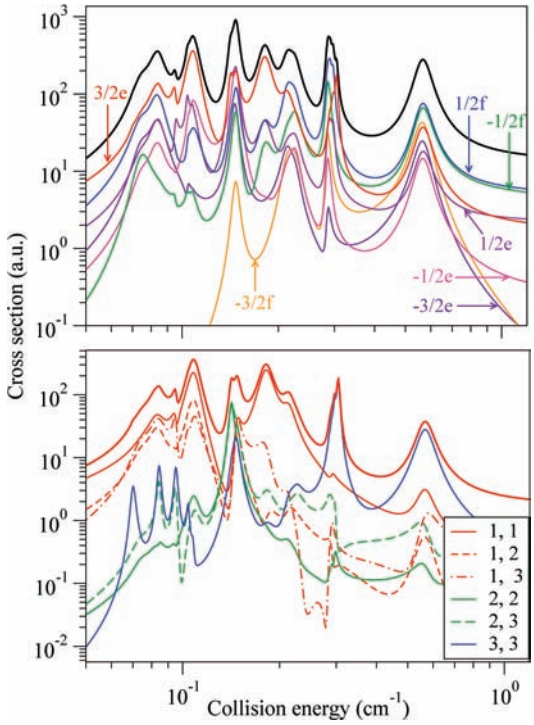

Figure 7. Same as Figure 6 but for an electric field of 5 kV/cm.

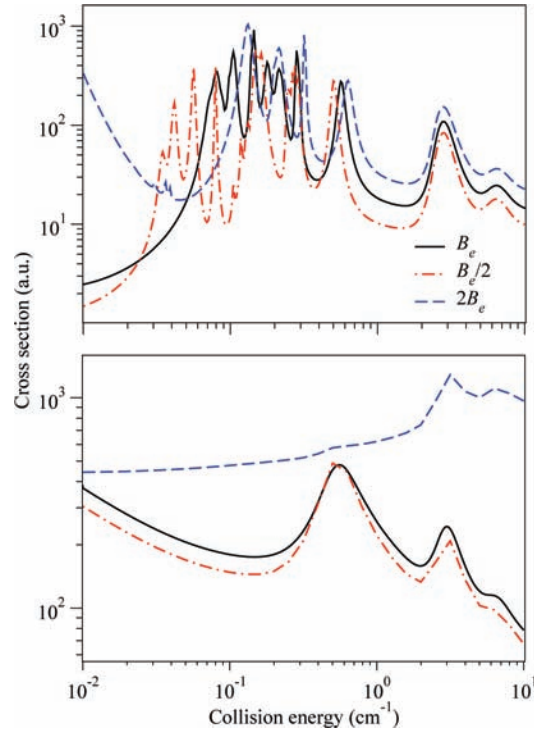

Figure 8. (upper panel) Collision energy dependence of the inelastic cross sections for OH (F_1, $J = 3/2$, $M = 3/2$, f) with He at an electric field of 5 kV/cm calculated with the rotational constant of OH multiplied by factors of 0.5 (dashed line) and 2 (dotted line). The original He−OH cross section (full line) is also shown for comparison. (lower panel) Same as the upper panel but for the OH molecules initially in the $|F_2$, $J = 1/2$, $M = 1/2$, $f\rangle$ state. The magnetic field is 1 G (upper panel) and 10^4 G (lower panel).

The electric-field-induced couplings of the opposite parity states lead to indirect couplings between different partial waves.[50] This, in turn, leads to the suppression of diagonal contributions to the scattering amplitude ($l \rightarrow l$) and enhancement of nondiagonal transitions ($l \rightarrow l \pm 1$).[50] As a result of these indirect couplings, many more partial waves become involved in the collision process and shape resonances get suppressed. As illustrated in the lower panel of Figure 7, the $l \rightarrow l \pm 1$ transitions result in many additional resonant contributions, which shift and split the individual resonance lines, leading to electric-field-induced resonance "broadening".

In order to explore the generality of our results, it is instructive to analyze the sensitivity of the cross sections to various parameters of the Hamiltonian (2). In Figure 8, we plot the total cross section for Stark relaxation in He−OH collisions from the $|F_1$, $J = 3/2$, $M = 3/2$, $f\rangle$ initial state calculated with the rotational constant of the OH molecule multiplied by factors of 0.5 and 2. Although the scaled cross sections exhibit a different resonant structure, the background value of the cross sections at $E_{coll} > 0.1$ cm^{-1} is not sensitive to the rotational constant. This confirms our previous conclusion[37] that M-changing transitions in $^2\Pi$ molecules occur via direct couplings of different Stark levels induced by the anisotropy of the interaction potential. As these couplings are typically strong, the collision dynamics of $^2\Pi$ molecules tends to be insensitive to their rotational structure.

To further illustrate this important point, we consider collisions of CH($^2\Pi$) molecules with He atoms in an electric field. We use the following spectroscopic constants for the CH radical[4] (in cm^{-1}): $A = 28.147$, $B_e = 14.192$, $p = 0.0335$, $q = 0.0287$, and $d = 1.46$ D.[51] The rotational constant of CH is very similar to that of OH, but the SO constant of CH is about 10 times smaller.[4] The upper panel of Figure 9 shows the lowest energy levels of CH as functions of the applied magnetic field. The levels correlating with the field-free state $|J = 1/2$, $\bar{\Omega} = 1/2$, $f\rangle$ have zero magnetic g-factors. The lower panel of Figure 9 shows that electric g-factors are not zero, so the CH molecules in the highest-energy Stark states can be decelerated and confined in an electrostatic trap.[16]

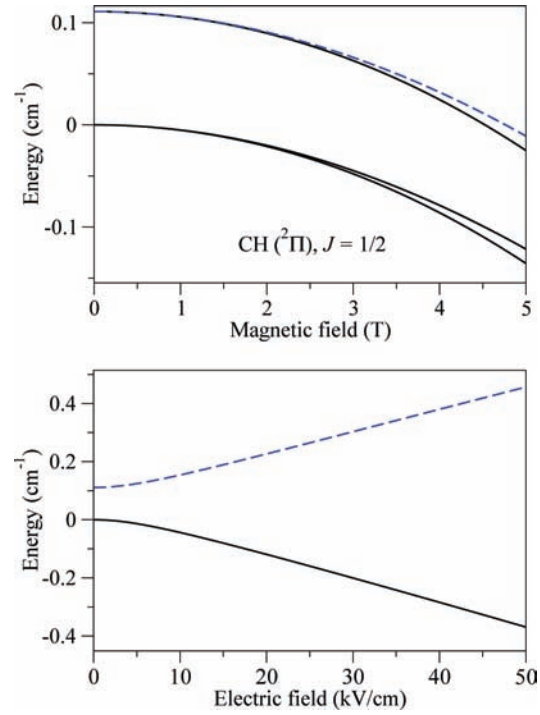

Figure 9. (upper panel) Magnetic field dependence of the lowest energy levels of CH at zero electric field. (lower panel) Electric field dependence of the lowest energy levels of CH at zero magnetic field.

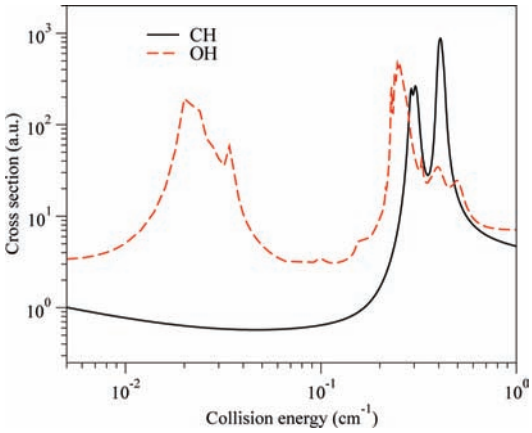

Figure 10. Collision energy dependence of the inelastic cross sections for CH ($J = 1/2$, $\bar{\Omega} = 1/2$, $M = 1/2$) (full line) and OH (F_1, $J = 3/2$, $M = 3/2$, f) (dashed line) with He at zero electric field. The magnetic field is 1 T (full line) and 0.5 T (dashed line).

Figure 10 shows the cross sections for M-changing transitions in collisions of CH molecules with He atoms calculated with the He−OH interaction potential. We note that the real He−CH interaction potential is more anisotropic than that for He−OH,[52] so the calculations presented in Figure 10 should not be regarded as quantitatively accurate. The inelastic cross sections for He−CH are large and similar to those for He−OH. The total inelastic cross sections for OH and CH agree well except for the broad peak at a collision energy of ~0.02 cm^{-1}. This peak corresponds to a shape resonance in the outgoing channel of OH, which is lower in energy than the initial channel due to the Zeeman splitting. Because the splitting is absent for CH ($J = 1/2$, $\bar{\Omega} = 1/2$, f) due to zero magnetic g-factors, the low-energy shape resonances do not occur in He−CH collisions. The results shown in Figure 10 demonstrate that varying the SO constant in $^2\Pi$ molecules does not alter the inelastic cross sections at collision energies above 0.2 cm^{-1}. The lack of specificity suggests that collisions of other $^2\Pi$ molecules with atoms may exhibit the same qualitative features.

C. Comparison with Experiment. In a recent experimental study, Sawyer et al. observed collisions of magnetically trapped OH molecules in the $|F_1, J = 3/2, M = 3/2, f\rangle$ initial state with a supersonic beam of ^{4}He atoms.[23] By analyzing the time dependence of trap loss, they were able to measure the absolute scattering cross sections at seven collision energies between 60 and 200 cm^{-1}. The measured cross sections displayed an interesting variation over a narrow interval of collision energies from 70 to 130 cm^{-1}, which was attributed to a threshold effect. As shown in Figure 2, the Λ-doublet components of the first rotationally excited state ($J = 5/2$) lie 83.9 and 84.1 cm^{-1} above the field-free ground state ($J = 3/2$). An electric field of 5 kV/cm further splits the components into six thresholds lying within 0.1 cm^{-1} of each other. According to the Wigner threshold law for s-wave scattering, the cross section for rotational excitation $J = 3/2 \rightarrow J' = 5/2$ should vary as $(E - E_{thr})^{1/2}$, where E_{thr} is the threshold energy and E is the total energy.[53]

In order to interpret the experimental findings,[23] we extended our quantum calculations to higher collision energies to obtain converged cross sections for elastic scattering and rotationally inelastic transitions in ^{4}He−OH collisions (throughout this section, we consider collisions with the ^{4}He isotope). The calculations were performed at the seven collision energies probed in the experiment.[23] To elucidate the role of inelastic transitions in He−OH collisions, we complemented the multichannel CC calculations with a simple model, which ignores

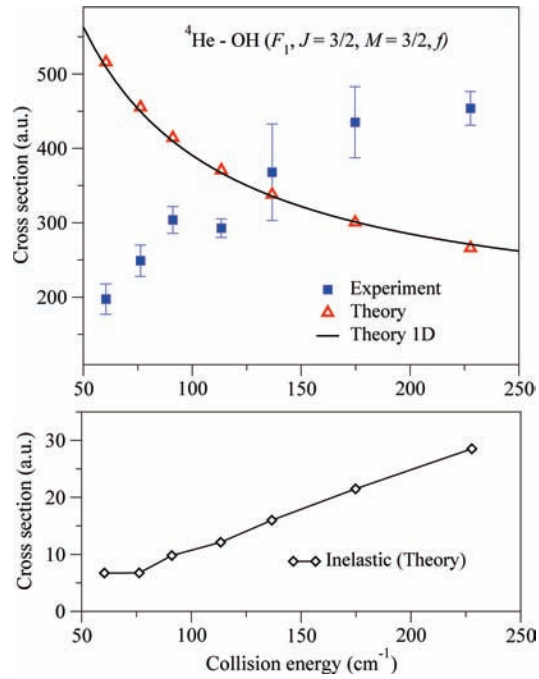

Figure 11. (upper panel) Total cross sections for ^{4}He−OH (F_1, $J = 3/2$, $M = 3/2$, f) as functions of collision energy: multichannel CC calculations (triangles), isotropic model (full line), experiment (squares with error bars). (lower panel) Collision energy dependence of the inelastic cross section for the same system from multichannel CC calculations. The electric field is 5 kV/cm, and the magnetic field is 1 G.

the anisotropy of the atom−molecule interaction potential. This approximation decouples the CC equations (10) to yield a set of one-dimensional (1D) Schrödinger equations, which we solve for a given partial wave l and collision energy E_{coll}. By summing the resulting partial cross sections over l, we obtain the total elastic cross section. To parametrize the 1D model, it is most natural to use the isotropic part of the atom−molecule interaction potential given by

$$V_0(R) = \int_0^\pi \frac{1}{2}[V_{A'}(R,\theta) + V_{A''}(R,\theta)] \sin\theta \, d\theta \quad (15)$$

where $V_{A'}(R,\theta)$ and $V_{A''}(R,\theta)$ are the He−OH interaction potentials of A' and A'' symmetry.[43] The 1D model has the advantage that scattering calculations based on it are less computationally intensive compared to the full multichannel CC calculations described in section II.

The upper panel of Figure 11 shows the calculated and measured total cross sections for collisions of OH molecules initially in the $|F_1, J = 3/2, M = 3/2, f\rangle$ state with He atoms at an electric field of 5 kV/cm. The calculated cross sections decrease monotonically with increasing collision energy, while the observed cross sections follow the opposite trend. At variance with experimental data, the calculated total cross sections display no threshold structure near E_{coll} ~84 cm^{-1}. However, the inelastic cross sections shown in the lower panel of Figure 11 do increase significantly as the collision energy is tuned across the $J = 5/2$ threshold. The absence of the threshold structure in the total cross section becomes clear when we compare the absolute magnitudes of the elastic and inelastic contributions: on average, the inelastic cross section accounts for less than 5% of the total cross section. The good agreement between the results of the 1D model and full multichannel CC

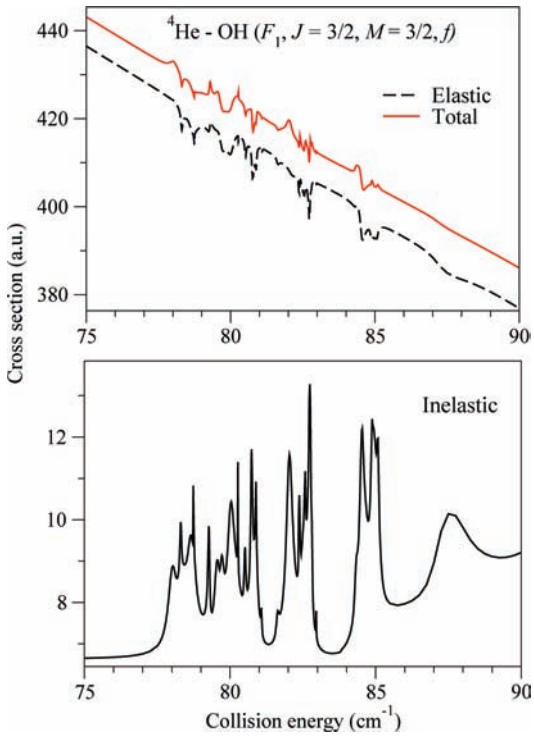

Figure 12. (upper panel) Calculated total (full line) and elastic (dashed line) cross sections as functions of collision energy near threshold. (lower panel) The inelastic cross section as a function of collision energy near threshold. Note the different *Y*-axis scaling for total and inelastic cross sections. The electric field is 5 kV/cm, and the magnetic field is 1 G.[38]

calculations shown in Figure 11 also suggests that the total cross section is dominated by the elastic contribution.

Figure 12 shows the cross sections for elastic and inelastic scattering in He−OH collisions calculated on a fine grid of collision energies in the vicinity of the $J = 5/2$ threshold. The complicated resonance structure in the lower panel of Figure 12 is due to the overlapping threshold dependencies of the cross sections for inelastic transitions from the rotationally ground state to the first rotationally excited state. As shown in Figures 11 and 12, the *total* cross section is dominated by elastic scattering, and hence shows little sensitivity to collision energy near threshold. These observations agree well with the previous experimental and theoretical studies of Xe−OH collisions near threshold based on multichannel CC calculations and accurate *ab initio* interaction potentials[22] calculated using the same *ab initio* method as the He−OH potentials used in this work. The calculations of Gilijamse et al. shown in Figure 3 of their paper[22] demonstrate that the inelastic cross section accounts for only a small fraction (<10%) of the total Xe−OH scattering cross section for collision energies from 50 to 300 cm^{-1}. In our calculations, this fraction is even smaller due to the weaker anisotropy of the He−OH interaction.

A possible source of the disagreement between theory and experiment may be traced to the He−OH interaction potentials used in scattering calculations. In order to explore the sensitivity of our results to variations of the interaction potential, we calculated the elastic cross sections with the isotropic term (15) multiplied by a constant scaling factor f_s. To avoid expensive multichannel calculations, we employed the 1D model to calculate the elastic cross sections as functions of collision energy for several values of f_s. The results presented in Figure 13 demonstrate that scaling the isotropic part of the interaction potential by factors of 0.5 and 1.5 modifies the magnitude of

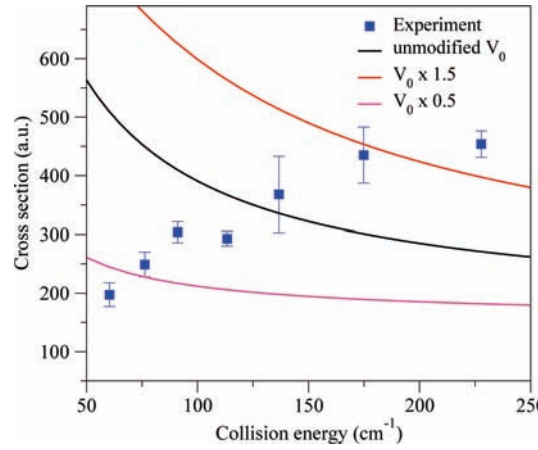

Figure 13. Same as the upper panel of Figure 11 but for the isotropic interaction potential multiplied by 0.5 (lower trace) and 1.5 (upper trace).

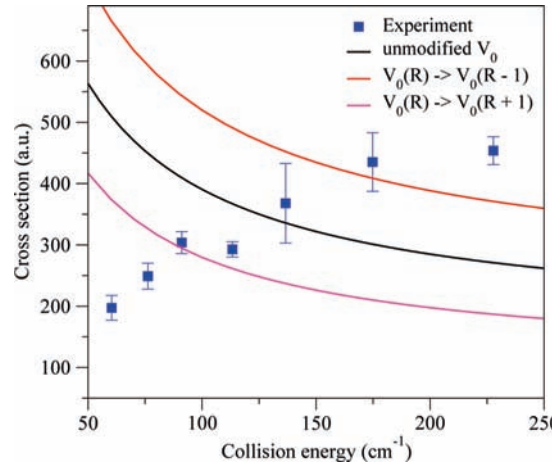

Figure 14. Same as the upper panel of Figure 11 but for the isotropic interaction potential shifted by 1 a_0 to the left (upper trace) and right (lower trace).

the cross sections but not their dependence on collision energy. The scaling factors chosen are large given the accuracy level typical of present-day *ab initio* interaction potentials (~10−20%). An independent calculation of the bound states of the He−OH van der Waals complex yielded good agreement with high-resolution spectroscopic measurements,[54] further supporting the reliability of the *ab initio* interaction potentials calculated by Lee et al.[43] We therefore believe that the uncertainties in our calculated cross sections are significantly smaller than shown in Figure 13 for $f_s = 0.5$ and 1.5.

The cross sections for elastic scattering are sensitive to the location of the repulsive wall of the interaction potential.[55] We performed calculations with the interaction potential shifted to smaller or larger R by 1 a_0. Figure 14 shows that these modifications do not affect the dependence of the cross sections on collision energy and the overall effect is very similar to that produced by scaling the interaction potential by a constant factor (see Figure 13). As with the scaling procedure mentioned above, shifting the interaction potential by 1 a_0 is a substantial modification that increases the rotational constant of the He−OH weakly bound complex by as much as 30% (the inaccuracy of the calculated rotational constants is normally on the order of a few percent).[43]

In conclusion, we have demonstrated that the total cross section for ^{4}He−OH is dominated by elastic scattering, which is a smooth function of collision energy near threshold (Figures

11 and 12). The robustness of this result to relatively large variations of the He−OH interaction potential (Figures 13 and 14) suggests that it is unlikely that the drop in the total cross section below 84 cm^{-1} observed by Sawyer et al.[23] results from a near-threshold variation of the inelastic cross section.

Very recently, Fagnan et al. measured the cross sections for collision-induced trap loss of cold Rb atoms in Ar buffer gas.[56] They showed that elastic collisions that result in forward scattering ($\theta < \theta_{min}$, where θ is the scattering angle) do not impart enough kinetic energy to the trapped Rb atoms to drive them out of the trap. The relative contribution of such "glancing collisions" depends on the trap depth, which determines the angular cutoff parameter θ_{min}. Because the differential cross sections for elastic scattering are strongly peaked near $\theta = 0$,[55] the observed cross sections for trap loss may be significantly smaller than those for elastic scattering,[56] which might explain some of the discrepancies shown in Figure 11.[57] A more detailed analysis of the effects of trap depth on He−OH scattering cross sections will be presented in a future publication.

IV. Summary

We have presented a theoretical analysis of He−OH collisions at low and ultralow collision energies based on rigorous quantum calculations of collision dynamics in the presence of external electromagnetic fields. We have shown that collision-induced Stark relaxation of OH molecules in the ground rotational state can be efficiently manipulated with electric fields of less than 30 kV/cm. The collision energy dependence of the inelastic cross sections is dominated by scattering resonances (Figure 3) whose positions and widths depend on the electric field strength. The complexity of the resonance structure increases with increasing field strength (Figures 6 and 7) due to the electric-field-induced couplings between the opposite parity states, which lead to indirect couplings between different partial waves. Resonances also occur in the electric field dependence of the inelastic cross sections at a fixed collision energy for the ground rotational state of OH. The cross sections for rotationally excited OH molecules in the F_1 and F_2 manifolds are smooth functions of collision energy (Figures 3 and 5).

At zero electric field, the OH molecules initially in the $|F_1, J = 3/2, M = 3/2, f\rangle$ state preferentially relax to the $|F_1, J = 3/2, M = 1/2, f\rangle$ state, illustrating the propensity rules for parity conservation and minimum change of M. However, these rules are not universal even in the absence of external fields, since other transitions may dominate depending on collision energy (Figure 6). Electric fields break these propensity rules completely, leading to population of all possible final channels with nearly equal probability (Figure 7). Electric fields also induce couplings between different partial waves, which leads to suppression of shape resonances, as shown in Figures 6 and 7. The magnitude of the inelastic cross section out of the $|F_1, J = 3/2, M = 3/2, f\rangle$ initial state increases 100-fold as the field strength is varied from 0 to 30 kV/cm. Rotational excitation of OH molecules opens up an additional pathway of rotational (J-changing) relaxation. The cross sections for J-changing transitions are typically a factor of 10 larger than those for Stark relaxation, and they are not sensitive to the electric field. The cross sections for fine-structure relaxation out of the $|F_2, J = 1/2, M = 1/2, f\rangle$ state are another 10 times larger (Table 2).

The results shown in Figures 11 and 12 demonstrate that the collision energy dependence of the total cross section for ^{4}He−OH is almost the same as that of the elastic cross section—the contribution from inelastic collisions amounts to less than 10%. This is further illustrated in the upper panel of Figure 12, which demonstrates good agreement between the results of a simple 1D model (which ignores the He−OH interaction anisotropy) and rigorous CC calculations. Although the inelastic cross section shows rapid oscillations as a function of collision energy near threshold (Figure 12), the variation of the total cross section over the same energy interval does not exceed 5%. On a wider scale, the calculated cross section decreases monotonically with collision energy. This is in contrast to the experimental results of Sawyer et al., who observed that the total cross section *increases* by ∼100% as the collision energy varies from 70 to 170 cm^{-1}. Figures 13 and 14 demonstrate that our calculated elastic cross sections are relatively robust against various artificial modifications of the isotropic part of the He−OH interaction potential. Test CC calculations show that multiplying the anisotropic part of the He−OH interaction potential by factors of 2−3 does not have any noticeable effect on the total cross sections. At present, the explanation for the observed energy dependence of the total cross section[23] is unclear, warranting further theoretical and experimental work.

Acknowledgment. We are grateful to Brian Sawyer and Kirk Madison for useful discussions. This work was supported by the Chemical Science, Geoscience, and Bioscience Division of the Office of Basic Energy Science, Office of Science, U.S. Department of Energy, and NSF grants to the Harvard-MIT Center for Ultracold Atoms and to the Institute for Theoretical Atomic, Molecular, and Optical Physics at Harvard University and Smithsonian Astrophysical Observatory.

References and Notes

(1) Summers, M. E.; Conway, R. R.; Siskind, D. E.; Stevens, M. H.; Offermann, D.; Riese, M.; Preusse, P.; Strobel, D. F.; Russell, J. M., III. *Science* **1997**, *319*, 1967.
(2) Atkinson, R. *Chem. Rev.* **1985**, *85*, 69.
(3) Dalgarno, A. *Faraday Discuss.* **2006**, *133*, 9.
(4) Brown, J.; Carrington A. *Rotational Spectroscopy of Diatomic Molecules*; Cambridge University Press: Cambridge, U.K., 2003.
(5) van Beek, M. C.; ter Meulen, J. J.; Alexander, M. H. *J. Chem. Phys.* **2000**, *113*, 628.
(6) van Beek, M. C.; ter Meulen, J. J.; Alexander, M. H. *J. Chem. Phys.* **2000**, *113*, 637.
(7) Marinakis, S.; Paterson, G.; Kłos, J.; Costen, M. L.; McKendrick, K. G. *Phys. Chem. Chem. Phys.* **2007**, *9*, 4414.
(8) Paterson, G.; Marinakis, S.; Costen, M. L.; McKendrick, K. G.; Kłos, J.; Toboła, R. *J. Chem. Phys.* **2008**, *129*, 074304.
(9) Brouard, M.; Bryant, A.; Chang, Y.-P.; Cireasa, R.; Eyles, C. J.; Green, A. M.; Marinakis, S.; Aoiz, F. J.; Kłos, J. *J. Chem. Phys.* **2009**, *130*, 044306.
(10) Komissarov, A. V.; Lin, A.; Sears, T. J.; Hall, G. E. *J. Chem. Phys.* **2006**, *125*, 084308.
(11) Jasper, A. W.; Zhu, C.; Nangia, S.; Truhlar, D. G. Non-adiabatic effects in chemical dynamics. *Faraday Discuss.* **2004**, *127*, 1.
(12) Suits, A. G.; Vasyutinskii, O. S. *Chem. Rev.* **2008**, *108*, 3706.
(13) Alexander, M. H.; Capecchi, G.; Werner, H.-J. *Science* **2002**, *296*, 715.
(14) van de Meerakker, S. Y. T.; Bethlem, H.; Meijer, G. *Nat. Phys.* **2008**, *4*, 595.
(15) Willitsch, S.; Bell, M.; Gingell, A.; Softley, T. P. *Phys. Chem. Chem. Phys.* **2008**, *10*, 7200.
(16) Bell, M. T.; Softley, T. P. *Mol. Phys.* **2009**, *107*, 99.
(17) Krems, R. V. *Phys. Chem. Chem. Phys.* **2008**, *10*, 4079.
(18) Weinstein, J. D.; deCarvalho, R.; Guillet, T.; Friedrich, B.; Doyle, J. M. *Nature* **1998**, *395*, 148.
(19) van de Meerakker, S. Y. T.; Vanhaecke, N.; Meijer, G. *Annu. Rev. Phys. Chem.* **2006**, *57*, 159.
(20) Lev, B. L.; Meyer, E. R.; Hudson, E. R.; Sawyer, B. C.; Bohn, J. L.; Ye, J. *Phys. Rev. A* **2006**, *74*, 061402(R).
(21) van de Meerakker, S. Y. T.; Vanhaecke, N.; van der Loo, M. P. J.; Groenenboom, G. C.; Meijer, G. *Phys. Rev. Lett.* **2005**, *95*, 013003.
(22) Gilijamse, J. J.; Hoekstra, S.; van de Meerakker, S. Y. T.; Groenenboom, G. C.; Meijer, G. *Science* **2006**, *313*, 1617.
(23) Sawyer, B. C.; Stuhl, B. K.; Wang, D.; Yeo, M.; Ye, J. *Phys. Rev. Lett.* **2008**, *101*, 203203.

(24) Lara, M.; Bohn, J. L.; Potter, D.; Soldán, P.; Hutson, J. M. *Phys. Rev. Lett.* **2006**, *97*, 183201.
(25) Lara, M.; Bohn, J. L.; Potter, D.; Soldán, P.; Hutson, J. M. *Phys. Rev. A* **2006**, *75*, 012704.
(26) Dagdidian, P.; Alexander, M. H. *J. Chem. Phys.* **2009**, *130*, 164315.
(27) Klar, H. *J. Phys. B* **1973**, *6*, 2139.
(28) Shapiro, M.; Kaplan, H. *J. Chem. Phys.* **1979**, *71*, 2182.
(29) Alexander, M. H. *J. Chem. Phys.* **1982**, *76*, 5974.
(30) Alexander, M. H.; Kearney, W. R.; Wagner, A. F. *J. Chem. Phys.* **1994**, *100*, 1338.
(31) Degli Esposti, A.; Berning, A.; Werner, H.-J. *J. Chem. Phys.* **1995**, *103*, 2067.
(32) Yang, X.; Dagdigian, P. J.; Alexander, M. H. *J. Chem. Phys.* **2000**, *112*, 4474.
(33) Avdeenkov, A. V.; Bohn, J. L. *Phys. Rev. A* **2002**, *66*, 052718.
(34) Avdeenkov, A. V.; Bohn, J. L. *Phys. Rev. Lett.* **2003**, *90*, 043006.
(35) Ticknor, C. T.; Bohn, J. L. *Phys. Rev. A* **2005**, *71*, 022709.
(36) González-Sánchez, L.; Bodo, E.; Gianturco, F. *Phys. Rev. A* **2006**, *73*, 022703.
(37) Tscherbul, T. V.; Groenenboom, G. C.; Krems, R. V.; Dalgarno, A. *Faraday Discuss.* **2009**, *142*, 127–141.
(38) Unless indicated otherwise, all calculations reported here are for a magnetic field of 1 G. Test calculations show that electric and magnetic fields have a negligible effect on scattering cross sections at collision energies above 60 cm^{-1}.
(39) Brown, J. M.; Kaise, K.; Kerr, C. M. L.; Milton, D. J. *Mol. Phys.* **1978**, *36*, 553.
(40) Brown, J. M.; Merer, A. J. *J. Mol. Spectrosc.* **1979**, *74*, 488.
(41) Krems, R. V.; Dalgarno, A. *J. Chem. Phys.* **2004**, *120*, 2296.
(42) Tscherbul, T. V.; Krems, R. V. *Phys. Rev. Lett.* **2006**, *97*, 083201.
(43) Lee, H.-S.; McCoy, A. B.; Toczyłowski, R. R.; Cybulski, S. M. *J. Chem. Phys.* **2000**, *113*, 5736.
(44) Alexander, M. H. *Chem. Phys.* **1985**, *92*, 337.
(45) Peterson, K. I.; Fraser, G. T.; Klemperer, W. *Can. J. Phys.* **1984**, *62*, 1502.
(46) Johnson, B. R. *J. Comput. Phys.* **1973**, *13*, 445.
(47) Manolopoulos, D. E. *J. Chem. Phys.* **1986**, *85*, 6425.
(48) Tscherbul, T. V.; Krems, R. V. *J. Chem. Phys.* **2006**, *125*, 194311.
(49) Hutson, J. M. *New J. Phys.* **2007**, *9*, 152.
(50) Tscherbul, T. V. *J. Chem. Phys.* **2008**, *128*, 244305.
(51) Phelps, D. H.; Dalby, F. W. *Phys. Rev. Lett.* **1966**, *16*, 3.
(52) Cybulski, S.; Chałasiński, G.; Szczęśniak, M. *J. Chem. Phys.* **1996**, *105*, 9525.
(53) Sadeghpour, H. R.; Bohn, J. L.; Cavagnero, M. J.; Esry, B. D.; Fabrikant, I. I.; Macek, J. H.; Rau, A. R. P. *J. Phys. B* **2000**, *33*, R93.
(54) Han, J.; Heaven, M. C. *J. Chem. Phys.* **2005**, *123*, 064307.
(55) Pauly, H. In *Atom-Molecule Collision Theory: A Guide for the Experimentalist*; Bernstein, R. B., Ed.; Plenum Press: New York, **1979**.
(56) Fagnan, D. E.; Wang, J.; Zhu, C.; Djuricanin, P.; Klappauf, B. G.; Booth, J. L.; Madison, K. W. *Phys. Rev. A*, in press.
(57) Sawyer, B.; Ye, J. Private communication.

JP904512R